ACS Symposium Series No. 874, "Polymers for Micro- and Nano-electronics," 2004, p. 86-97

Correlation of the Reaction Front with Roughness in Chemically Amplified Photoresists

Ronald L. Jones[1], Vivek M. Prabhu[1], Darío L. Goldfarb[3], Eric K. Lin[1], Christopher L. Soles[1], Joseph L. Lenhart [1,2], Wen-li Wu[1], and Marie Angelopoulos[3]

[1] Polymers Division, National Institute of Standards and Technology, Gaithersburg, MD 20899-8541,
[2] Current address: Sandia National Laboratories, NM
[3] IBM T.J.Watson Research Center. Yorktown Heights, NY 10598

RESERVE THIS SPACE

ACS Symposium Series No. 874, "Polymers for Micro- and Nano-electronics," 2004, p. 86-97

Abstract

A model bilayer geometry is used to correlate the reaction front profile width with roughness after development in 0.26 N tetramethylammonium hydroxide aqueous base developer. The bilayer geometry utilizes a bottom layer of protected photoresist polymer with a top layer of deprotected photoresist loaded with photoacid generator. Neutron reflectivity measurements show that the reaction front profile broadens during post-exposure bake (PEB) times between 15 s and 90 s to a width approaching 150 Å. The subsequent development and atomic force microscopy experiments reveal an increase in nominal root-mean-squared (RMS) roughness as well as increased lateral length scale features with PEB time. While the form and size of the deprotection profile have been proposed as an important factor in line edge roughness (LER) formation, this study shows the connection of sidewall morphology to a measured deprotection profile.

Introduction

The influence of photogenerated acid diffusion on side-wall or line-edge roughness (LER) is an increasingly important problem for photoresist imaging. The push to reduce feature widths to dimensions on the order of 30 nm in the next decade, where tolerances are typically on the order of (1 to 5) %, dictates a reduction of LER tolerance to sub-nanometer levels (1). In addition to effects arising from optical blurring in the image projection (2-5), material factors contributing to LER include acid diffusion (6-8), photoresist chemistry (9,10), and developer characteristics (11). Formation of the line edge occurs through a process that includes projection of an optical mask image on a polymer-based thin film containing a photosensitive small molecule, termed a photoacid generator (PAG). Upon exposure, the photogenerated acid deprotects the polymer matrix, forming a base-soluble matrix that is selectively removed by a developer solution. The line edge is therefore created at an internal interface

between protected and deprotected species. The factors contributing to LER can therefore be grouped into factors that define the internal deprotection interface (i.e. image blur, acid diffusion) and factors defining the selectivity of the dissolution process (i.e. developer concentration, photoresist/developer interaction). Recent work by our group has demonstrated an ability to measure this interface directly under normal processing conditions (12), along with ongoing studies of the early time dependence of the root mean square (RMS) roughness (13). The RMS roughness is observed to increase during early times, reaching a plateau. In this work, we probe the limit of small image blur to provide data directly connecting the breadth of the deprotection profile interface to the final surface morphology. The morphology is characterized by the lateral correlations of RMS, or the scan size dependence of RMS, rather than the total value of roughness.

To facilitate measurements of the deprotection profile, we follow a procedure outlined previously to produce a model pattern "sidewall" as a top surface (12-14). Here, the line edge of a chemically amplified resist is modeled using a bilayer prepared with a bottom layer of protected polymer and a top "feeder" layer of deprotected polymer loaded with PAG. Upon blanket exposure, the photogenerated acid diffuses across the interface, generating an interfacial profile of deprotected species that increases in width with post exposure bake (PEB) time. This study represents a direct experimental connection of the deprotection profile caused by acid diffusion and reaction to the final surface morphology. The profile is measured using high resolution neutron (NR) and x-ray (XR) reflectivity, while the surface morphology is characterized using atomic force microscopy (AFM).

Experimental

Materials

Bilayer structures were prepared on cleaned silicon wafers (approximately 3 mm thick and 75 mm diameter) as follows: 5 min exposure to oxygen plasma, followed by removal of native oxide layer by immersion into a solution of (10 ± 2) % volume fraction HF and (5 ± 2) % volume fraction NH_3F in ultra pure water for (15 ± 5) s. An oxide layer was regrown in a UV/Ozone chamber for (120 ± 1) s followed by priming with hexamethyldisilazane vapor (HMDS). The lower layer consisting of the deutero-poly(butoxycarboxy styrene) (d PBOCSt) ($M_{r,n}$ = 21000, $M_{r,w}/M_{r,n}$ = 2.1) was spin-coated from a propylene

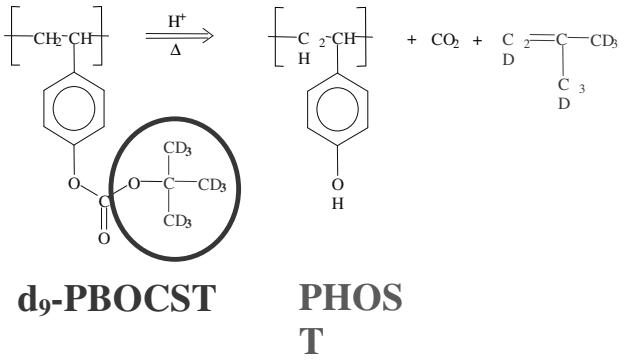

Figure 1. Schematic of the deprotection reaction showing the protected polymer, PBOCSt, and deprotected analog, PHOSt. Shown encircled is the protecting group cleaved by the photogenerated acid.

glycol methyl ether acetate (PGMEA) solution and post-apply baked (PAB) for 90 s on a 130 °C hotplate to remove residual solvent. The corresponding deprotected polymer, poly(hydroxystyrene) (PHOSt) ($M_{r,n}$ = 5260, $M_{r,w}/M_{r,n}$ = 1.12), was spin-coated from a 1-butanol solution directly onto the lower layer. The PHOSt layer is loaded with a 5 % mass fraction of the photoacid generator, di(*tert*-butylphenyl) iodonium perfluorooctanesulfonate. The bilayer is subjected to another PAB for 90 s at 130 °C. The model bilayer stack was exposed with a broadband UV dose of ≈1000 mJ/cm^2 to generate acid within the top PHOSt layer followed by PEB at 110 °C for varying times of 15 s, 20 s, 30 s, and 90 s. The original PHOSt layer and the soluble deprotected d-PBOCSt reaction products were removed (developed) by immersion in a 0.26 N tetramethylammonium hydroxide (TMAH) solution for 30 s followed by a rinse with deionized water. The use of deuterated PBOCSt facilitates the measurement of the deprotection profile using neutron reflectometry, described below. The approximate deprotection reaction of d-PBOCSt into PHOSt is shown schematically in figure 1.

Neutron Reflectivity

The bilayer samples were measured both before and after aqueous base development by specular neutron reflectivity (NR) on the NG7 reflectometer at the National Institute of Standards and Technology Center for Neutron Research. The NR experiments measure the specular reflected intensity, such that the angle

of incidence equals the angle of reflectance that defines a scattering wavevector q ($q= 4\pi\lambda^{-1}\sin(\theta/2)$), where λ is the neutron wavelength of 4.75 Å and θ is the angle of reflectance. The deprotection profile is then extracted from the data using a common modeling procedure. The details of these measurements are provided in a prior publication (12).

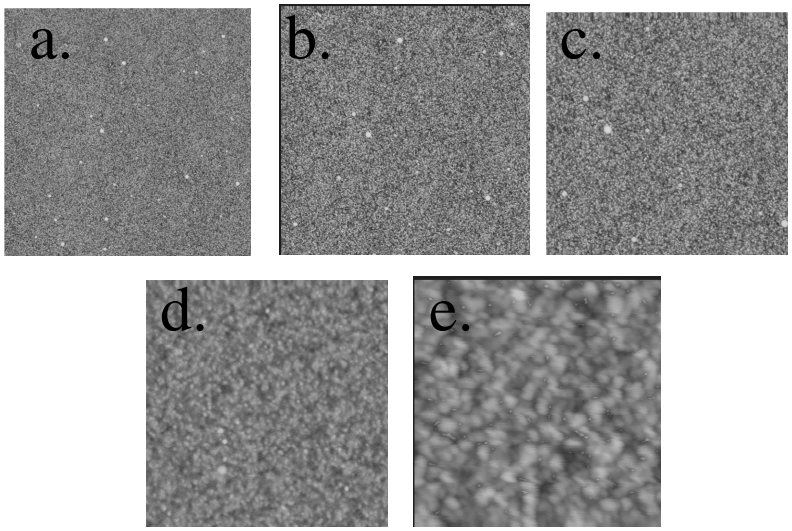

Figure 2. AFM tapping-mode images as function of scan size: (a) 10 x 10 μm, (b) (5 x 5) μm , (c) (2 x 2) μm, (d) (1 x 1) μm , (e) (0.5 x 0.5) μm , for a random copolymer o fPHOSt with 20 % mass fraction PBOCSt (No PAG) No PAB, 0.14 N TMAH for 30 s.

Atomic Force Microscopy

The surface image of all samples was measured using a Digital Dimension 3000 atomic force microscope (AFM) in tapping mode. The acquired images were corrected with a plane-fit. RMS roughnesses were obtained using the DI software. As in prior reports (15), the RMS roughness was found to be scan-size dependent. Therefore, the morphology is characterized here using the Fourier components of the image. Fourier transformations of multiple topographic images were found to be isotropic in 2-dimensions and subsequently circularly averaged into a 1-D spectrum. These spectra were averaged to provide a statistical average over a large area of the sample. The final power spectrum provides the lateral structure, in which the image is understood in terms of the

probability amplitude of lateral-length scale correlations versus wavevector, q (= 2π/d, where d is a real space length scale). A complete power spectrum covering two-decades of length scale information, was prepared by superposition of Fourier-transform images of different AFM scan sizes ranging from (0.5 μm x 0.5 μm) to (10.0 μm x 10.0 μm). Discrete Fourier transforms often result in large uncertainty near summation limits due to sampling errors, finite size, and the pixel dimensions. In an effort to determine the appropriate range of

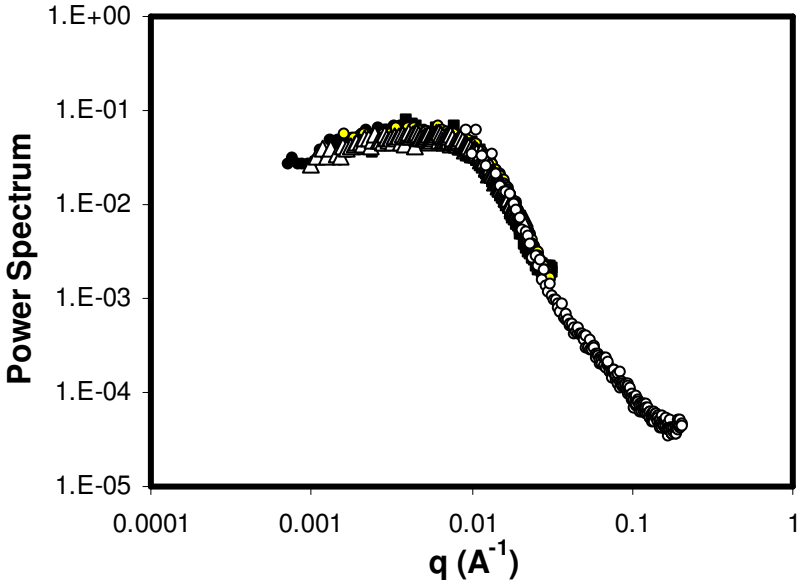

Figure 3. Fourier transform of images shown in figure 2 as function of scan size. Data shown outline the limits of q used for each scan size in this study.

wavevector for each scan size, a test film of a random copolymer of PHOSt with 20 % mass fraction PBOCSt was partially developed in 0.14 N TMAH and imaged (see figure 2). As shown in figure 3, Fourier transforms from 5 different scan sizes were then overlaid. By selecting ranges of Q where two overlapping data sets agreed to ± 20 % of the power spectral intensity, limits of minimum and maximum Q were established for each scan size. In this report, quantitative analysis of the power spectral intensity is not utilized, and therefore the intensity is arbitrarily shifted for clarity in the figures. The relative intensities within a scan have a maximum relative uncertainty of ± 20 % at low q values, with substantially smaller errors as q increases.

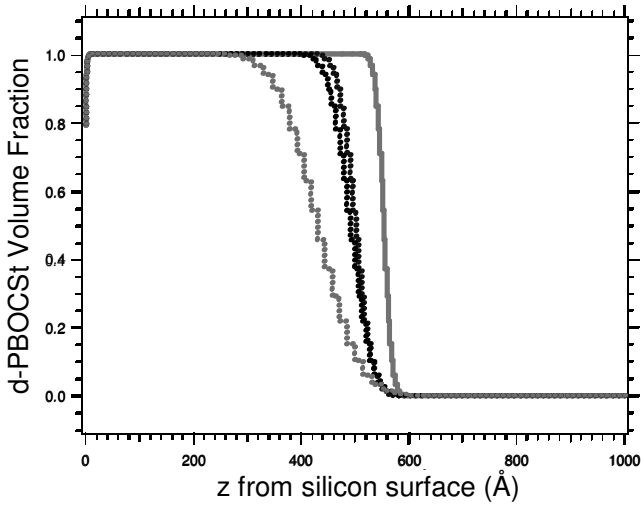

Figure 4. Neutron reflectivity results of reaction front profile Shown are the volume fraction of protected polymer (PBOCSt) as a function of distance from the substrate, z, for varying PEB times. Curves progress left with increasing PEB time, with the earliest (30 s) shown as a solid line, followed by data from 30 s, 60 s, and 90 s (dotted lines).

Results and Discussion

Reaction Front Profile

The reflectivity experiments are sensitive to gradients in the scattering length density of the thin film. For the case of NR, the deuterated protecting group has a different scattering length density than the top layer of protonated PHOSt. This scattering length density difference will lead to the ability to probe the deuterium labeled species composition profile. This is contrasted with XR, which measures differences in electron density, for which the density difference

is insufficient to measure the bilayer structure. From model fitting of scattering length density profiles, we are able to measure the fraction of protected species throughout the film thickness for the case of NR, while for XR a single layer of average electron density adequately fits the data (see figure 4). In this paper, we restrict our discussion to the effect of the internal, or pre-developed, interfacial deprotection profile on the resulting roughness observed after development. The details of the internal and developed NR and XR experimental data and reaction kinetics are outside the scope of this paper and will be presented elsewhere.

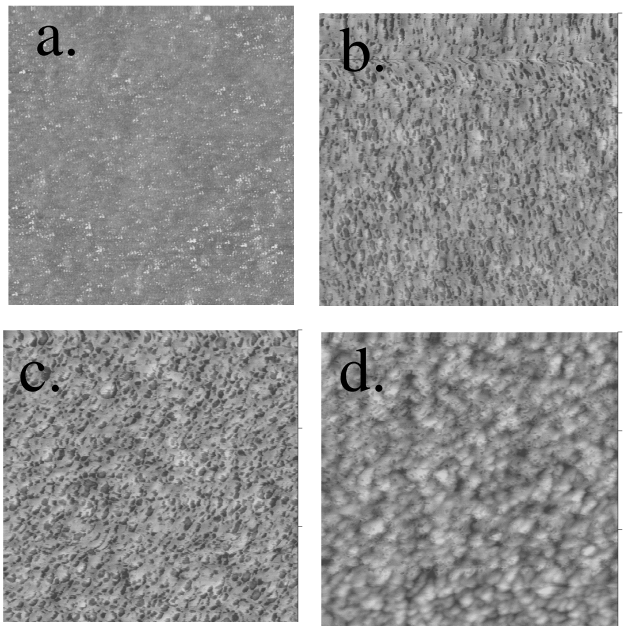

Figure 5. Tapping-mode AFM images from samples measured in figure 4. Shown are samples with PEB times of: (a) 0 s, (b) 15 s, (c) 30 s, (d) 90 s

Developed Surface Morphology

After the development of the bilayers of different PEB times, we measured the surface morphology using AFM. The surface images are presented in Fig. 5. The topographic images illustrate increased lateral structure during the initial

stages of reaction front propagation. The result is a continuous progression from an intially featureless surface, with an RMS roughness less than 1 nm, to a nodular structure with an RMS roughness of [3.1 ± 0.5] nm. The nodular morphology is found to persist without significant change for all PEB times greater than 90 s. Similar morphologies have been reported at the line edge of patterned photoresists (2,13). With only a limited number of points, the time evolution of the RMS roughness is not addressed further here. Instead, the morphology is characterized through lateral correlations of height.

The Fourier transform imaging quantifies the increase in lateral inhomogeneity through a characteristic wave vector, labeled here as Q*. The form of the data in figure 5 is similar to that found in studies of homopolymer surfaces, where a power law dependence at large Q transitions to a plateau at low Q vectors. Using a two regime representation, the transition between power law and plateau behavior occurs over a region centered at Q*. The value of Q* then signifies a characteristic length scale of the nodular structure observed in figure 4. In figure 6, a shift of Q*, signified by a the characteristic "knee" in the logarithmic power spectral density, to lower values of Q is observed with increasing PEB time. Further increases in PEB time did not result in significant changes in Q*.

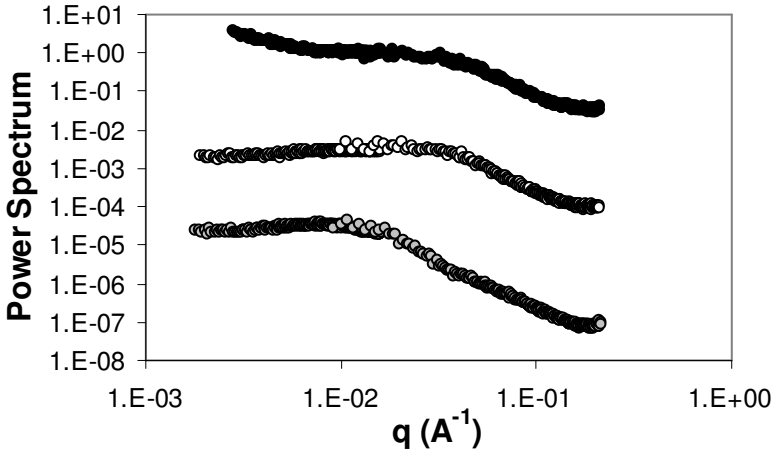

Figure 6. Fourier transform of topographic data from figure 5. Shown are data from PEB of 15 s (top), 30 s (middle), and 90 s (bottom).

Reaction-Front Width and RMS roughness

A composite plot of the reaction front profile width and RMS roughness as functions of the PEB time are shown in Fig. 7. This provides the opportunity to correlate the increased observed surface roughness with the development of an increasingly broadened reaction front profile. The deprotection profile widths range from an intially sharp interface of 20 Å to a broadened 140 Å. However, the development of this internal interface leads to RMS roughness of only (10 to 25) Å. Thus, design criteria for PEB processing that minimizes compositional broadening could serve as a controllable goal to minimize LER.

We should emphasize that the origin of the observed increase in surface roughness reflects a result consistent with true line-edge roughness. Fig. 8 provides a schematic of the types of interface geometries used to understand LER. The first is the typical single layer method in which either a blend or resist formulation is examined for roughness after typical wafer processing. Partially developing a uniform film would not include the interaction of the developer with the reaction front gradient. The second geometry is of the type used in this

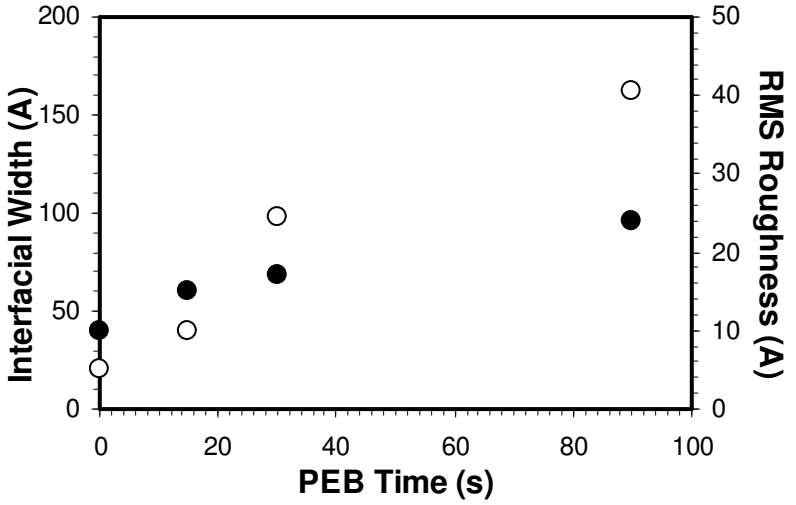

Figure 7. Composite plot of neutron reflectivity reaction front interfacial width (open circles) and AFM RMS roughness (filled circles) versus post-exposure bake time. PEB temperature is 110 °C. AFM roughness values have a relative uncertainty of ± 2 nm, while the deprotection profile width has a relative uncertainty of ± 3 nm.

work. The use of a bilayer to create a gradient is similar in scope to efforts to create gradients using an exposure wavelength that cannot fully penetrate the resist film. The advantage of the bilayer is the ability to create well defined starting points suitable to studies where image blur is considered negligible compared to the effects of acid diffusion. The last experimental method involves the creation of a true line edge. While this case is the most relevant to semiconductor processing, it is the least convenient geometry to measure. Only in the last two geometries are composition gradients present.

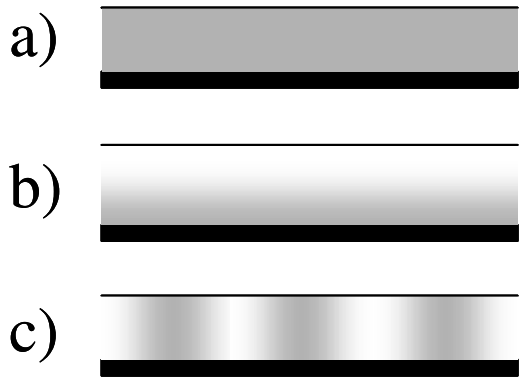

Figure 8. Model film geometries to study photoresist roughness. (a) Single layer with resist and/or blend of protected and deprotected components with additives. (b) This work, bilayer with deprotected bottom layer and top deprotected PAG feeder layer. (c) True profile prepared with mask to study resist performance.

The movement of the lateral length scale observed by AFM with the deprotection profile width is consistent with the model proposed by Schmid et al. (16). Here, the spatial distribution of deprotection is in great part a determining factor of the final line edge morphology. As the deprotection profile width increases, the level of inhomogeneity experienced by the developer may also increase, resulting in a larger length scale of line edge roughness. Other workers have attributed similar forms of line edge morphology to polymer aggregates present in chain scission resists during the developing step (17, 18). In our experiments, the evolution of the surface morphology follows the development of the reaction front. This evolution is not entirely consistent with preformed aggregates. However, in our case the reaction front width of 140 Å does not exceed the lateral scale morphology, thus we can not rule out that such aggregation could exist, or be enhanced by the development process.

Conclusions

The magnitude of lateral correlations in average line edge, or sidewall, roughness was measured as a function of the size of the deprotection profile width. As the deprotection profile broadens during the initial stages of post exposure baking, both the overall size of the RMS roughness and the characteristical lateral length scale defining the morphology were found to increase. For PEB times longer than 90 s at 110 °C, the characteristic length reaches a plateau and becomes invariant with PEB time (11). The dependence on deprotection profile width complements prior reports of the PEB time dependence of RMS roughness, suggesting a mechanism of lateral correlation development and RMS roughness.

Acknowledgements

This work was supported by the Defense Advanced Research Projects Agency under grant N66001-00-C-8803 and the NIST Office of Microelectronics Programs. J.L.L and V.M.P. acknowledge support through the National Research Council-National Institute of Standards and Technology Postdoctoral Fellowship Program. The authors would like to thank David R. Medeiros for the synthesis of h-PBOCST, B.C. Trinque, S. D. Burns, and C. G. Willson for the synthesis of d_9-PBOCST and R.W. Kwong for the GPC measurements.

References

1. *2001 National Technology Roadmap for Semiconductors*, The Semiconductor Industry Association: San Jose, CA (2001).
2. G. W. Reynolds, J. W. Taylor, J. Vac. Sci. Technol. B. **17**, 334 (1999).
3. G. P. Patsis, N. Glezos, I. Raptis, E. S. Valamontes, J. Vac. Sci. Technol. B. **17**, 3367 (1999).
4. W. D. Hinsberg, F. A. Houle, M. I. Sanchez, G. M. Walraff, IBM J. Res. & Dev. **45**, 667 (2001)
5. F. A. Houle, W. D. Hinsberg, M. I. Sanchez, Macromolecules **35**, 8591 (2002).
6. G. M. Schmid, M. D. Smith, C. A. Mack, V. K. Singh, S. D. Burns, C. G. Willson, Proc. SPIE **3999**, 675 (2000).
7. Y.-S. Kim, Y.-H. Kim, S. H. Lee, Y.-G. Yim, D. G. Kim, J.-H. Kim, Proc. SPIE **4690**, 829 (2002).
8. M. Yoshizawa, S. Moriya, J. Vac. Sci. Technol. B. **20**, 1342 (2002).
9. Q. Lin, R. Sooriyakumaran, W.-S. Huang, Proc. SPIE **3999**, 230 (2000).
10. Q. Lin, D. L. Goldfarb, M. Angelopoulos, S. R. Sriram, J. S. Moore, Proc. SPIE **4345**, 78 (2001).
11. L. W. Flanagin, V. K. Singh, C. G. Willson, J. Vac. Sci. Technol. B. **17**, 1371 (1999).
12. E. K. Lin, C. L. Soles, D. L. Goldfarb, B. C. Trinque, S. D Burns, R. L. Jones, J. L. Lenhart, M. Angelopoulos, C. G. Willson, S. K. Satija, W.-L. Wu, Science, **297**, 372 (2002).
13. D. L. Goldfarb et al., in preparation (2002).
14. D. L. Goldfarb, M. Angelopoulos, E. K. Lin, R. L. Jones, C. L. Soles, J. L. Lenhart, W.-L. Wu, J. Vac. Sci. Technol. B. **19(6)**, 2699 (2001).
15. D. He, F. Cerrina, J. Vac. Sci. Technol. B **16**, 3748 (1998)
16. G. M. Schmid, M. D. Smith, C. A. Mack, V. K. Singh, S. D. Burns, C. G. Willson, Proc. of the SPIE **4690**, 381 (2002).
17. T. Yamaguchi, H. Namatsu, M. Nagase, K. Yamazaki, K. Kurihara, Appl. Phys. Lett. **71**, 2388 (1997).
18. T. Yoshimura, H. Shiraishi, J. Yamamoto, S. Okazaki, Appl. Phys. Lett. **63**, 764 (1993).